Intrinsic Electrophysiology of Mouse Corticospinal Neurons: a Class-Specific Triad of Spike-Related Properties

Benjamin A. Suter[1], Michele Migliore[2] and Gordon M.G. Shepherd[1]

[1]Department of Physiology, Feinberg School of Medicine, Northwestern University, Chicago, IL 60611, USA and [2]Institute of Biophysics, National Research Council, Palermo 90146, Italy

Address correspondence to Gordon M.G. Shepherd, Morton 5-660, 303 E. Chicago Ave., Chicago, IL 60611, USA.
Email: g-shepherd@northwestern.edu

Corticospinal pyramidal neurons mediate diverse aspects of motor behavior. We measured spike-related electrophysiological properties of identified corticospinal neurons in primary motor cortex slices from young adult mice. Several consistent features were observed in the suprathreshold responses to current steps: 1) Corticospinal neurons fired relatively fast action potentials (APs; width at half-maximum 0.65 ± 0.13 ms, mean ± standard deviation [SD]) compared with neighboring callosally projecting corticostriatal neurons. Corticospinal AP width was intermediate between 2 classes of inhibitory interneuron in layer 5B. Spike-to-spike variability in AP width and other spike waveform parameters was low, even during repetitive firing up to 20 Hz, that is, the relative narrowness of corticospinal APs was essentially frequency independent. 2) Frequency–current (f–I) relationships were nearly linear. 3) Trains of APs displayed regular firing, with rates typically staying constant or accelerating over time. Corticospinal neurons recorded from older mice (up to 4 months) or from a separate lateral cortical area (Region B; corresponding to secondary somatosensory cortex) showed generally similar intrinsic properties. Our findings have implications for interpreting spike waveforms of in vivo recorded neurons in the motor cortex. This analysis provides a framework for further biophysical and computational investigations of corticospinal neurons and their roles in motor cortical function.

Keywords: action potential, corticospinal, corticostriatal, electrophysiology, motor cortex

Introduction

Corticospinal neurons are pyramidal neurons in neocortical layer 5B that project directly to the spinal cord (Betz 1874; Phillips and Porter 1977). An understanding of the functional organization of the motor cortex entails knowledge of how these primary output neurons process inputs and transmit commands. Recently, in a series of brain slice experiments, we have examined the synaptic organization of mouse motor cortex. Retrograde labeling methods, in particular, have facilitated characterization of microcircuits conveying local excitation to corticospinal neurons (Anderson et al. 2010; Kiritani et al. 2012). Analysis of subthreshold intrinsic properties showed that corticospinal neurons express high levels of hyperpolarization-activated cyclic nucleotide-gated cation channels and hyperpolarization-activated current (H current; I_h), and evidence pointed to a role for I_h in modulating the efficacy of synaptic and dendritic integration in corticospinal neurons, particularly the conversion of local excitatory synaptic input into spiking output (Sheets et al. 2011).

In the course of these prior studies, we noticed distinctive properties of the action potentials (APs) of corticospinal neurons. In particular, corticospinal APs appeared faster (narrower; shorter in duration) compared with other projection neurons, even during repetitive firing. Fast APs have previously been noted for subsets of large layer 5 pyramidal neurons in both cat (Dykes et al. 1988; Spain et al. 1991a; Chen et al. 1996a, 1996b) and primate (Chen and Fetz 2005) motor cortex. Indeed, recently it has been reported that pyramidal tract-type neurons in primate motor cortex, presumed to be large corticospinal neurons, fire very fast ("thin", narrow) spikes (Vigneswaran et al. 2011). Corroborating these electrophysiological observations is anatomical evidence that Betz cells (presumed corticospinal neurons) in primate motor cortex express high levels of A-type Kv3 potassium channels (Ichinohe et al. 2004), which speed AP repolarization and thereby shorten AP duration (Rudy and McBain 2001). However, the extent to which the intrinsic properties of corticospinal neurons are conserved across or even within species is not clear. In rats, for example, the intrinsic properties of corticospinal neurons have been noted to be heterogeneous (Tseng and Prince 1993).

The aim of this study was to quantify the AP-related properties of mouse corticospinal neurons. We performed whole-cell recordings from retrogradely labeled neurons in brain slices of motor cortex prepared from mice at approximately 1 month of age. For comparison, we recorded from corticostriatal neurons and interneurons in the same sublayer. We also analyzed data sets obtained from mice up to 4 months of age, to assess possible age-dependent changes, and from corticospinal neurons located in a separate, lateral cortical area. Our findings indicate that mouse corticospinal neurons possess a characteristic set of AP-related properties.

Materials and Methods

Animals

The animal studies were approved by the Animal Care and Use Committee of Northwestern University. Most experiments (all those involving recordings from corticospinal or corticostriatal neurons) were performed using wild-type mice (strain: C57Bl/6J; The Jackson Laboratory). In the experiments involving recordings from interneurons, we used GAD67-GFP (line G42; CB6-Tg(Gad1-EGFP)G42Zjh/J) mice (Chattopadhyaya et al. 2004) or GIN (FVB-Tg(GadGFP)45704Swn/J) mice (both from The Jackson Laboratory) (Oliva et al. 2000).

Retrograde Labeling

The mice underwent stereotaxic injections of retrograde tracers (fluorescent microspheres; green or red RetroBeads from Lumafluor; Katz et al. 1984) at postnatal day (P) 21 or later, following previously described methods (Tseng et al. 1991; Akintunde and Buxton 1992; Anderson et al. 2010). They were deeply anesthetized (inhaled

isoflurane), placed in a stereotactic frame, and thermally supported by a feedback-controlled heating pad. An analgesic (buprenorphine) was administered at the start of the surgery. To label corticospinal neurons, an incision was made into the scalp and skin over the cervical spinal cord, the vertebrae were exposed using retractors, and a laminectomy was performed at the C2 level. A glass pipette was advanced through the dura just lateral to the midline to a depth of 1 mm; the retrograde tracer was pressure injected (Picospritzer III, Parker Hannifin) at 3–4 successively shallower depths (up to ∼0.2 mm). To label corticostriatal neurons (specifically, "crossed" corticostriatal neurons, i.e., intra-telencephalic type corticostriatal neurons projecting through the corpus callosum to the contralateral hemisphere), we pressure-injected the retrograde tracer unilaterally to the dorsolateral striatum (0.0 mm posterior, 2.0 mm lateral, 2.5 mm ventral to bregma), using an oblique approach to minimize labeling of corticocortical axons. After retracting the pipette slowly, the surgical wound was closed with adhesive.

Slice Preparation

Coronal brain slices containing the motor cortex were prepared 1–10 days after surgery (P23–32 for the primary data set, P42–110 for age comparisons), as described (Anderson et al. 2010). The animals were deeply anesthetized with isoflurane gas and decapitated. The head was immediately placed into ice-cold cutting solution (in mM: 110 choline chloride, 11.6 sodium L-ascorbate, 3.1 pyruvic acid, 25 $NaHCO_3$, 25 D-glucose, 2.5 KCl, 7 $MgCl_2$, 0.5 $CaCl_2$, 1.25 NaH_2PO_4; aerated with 95% O_2/5% CO_2) and the brain dissected. For optimal preservation of apical dendrites within slices of the targeted region, a coronal blocking cut was made with the razor blade tilted 10° rostrally. Coronal slices (300 µm thick), containing the region of mouse motor cortex with lowest thresholds for evoking forelimb movements by intracortical stimulation (Li and Waters 1991; Weiler et al. 2008; Ayling et al. 2009; Tennant et al. 2011; Hooks et al. 2011), were prepared on a vibratome (VT 1200S; Leica). The slices were transferred to artificial cerebrospinal fluid (ACSF, in mM: 127 NaCl, 25 $NaHCO_3$, 25 D-glucose, 2.5 KCl, 1 $MgCl_2$, 2 $CaCl_2$, 1.25 NaH_2PO_3; aerated with 95% O_2/5% CO_2) and maintained at 34°C for 30 min. The slices were then returned to room temperature for at least 30 min prior to recording.

Electrophysiology

The brain slices were transferred to the recording chamber of an upright microscope (BX51WI; Olympus) equipped with a cooled video camera (Retiga 2000R; QImaging), and superfused with recirculating aerated ACSF warmed to 34°C via a feedback-controlled heater (TC 324B; Warner). Bright-field gradient contrast microscopy was performed using an infrared light-emitting diode (LED, M850L2; Thorlabs). Epifluorescence microscopy was performed using LED illumination (M470L, M530L2; Thorlabs) and standard filter sets (U-N31002, U-N41017; Chroma). The slices were visualized and positioned using a low-magnification objective lens (UPlanSApo 4×/0.16; Olympus), to select a region containing retrogradely labeled cell bodies in layer 5B (contralateral to the injection site). Individual labeled neurons were identified using a high-magnification water immersion objective lens (LUMPlanFL N 60×/1.00; Olympus) and targeted for somatic whole-cell recordings. Patch pipettes were pulled (P-97; Sutter) from borosilicate glass (inner diameter 0.86, outer diameter 1.50 mm, with filament; Warner) to a tip resistance of 2–4 MΩ. Whole-cell recording configuration was obtained using a micromanipulator (MP-225, ROE-200, MPC-200; Sutter) and a patch-clamp amplifier (Multiclamp 700B; Axon Instruments). Pipette capacitance was compensated for before breaking in, and in current-clamp mode, the bridge was balanced periodically using the auto-adjust feature. Series resistance was monitored periodically in voltage-clamp mode by brief negative steps, and recordings were terminated if it exceeded approximately 25 MΩ.

Recordings were made in current-clamp mode with (except where noted) a potassium-based internal solution (in mM: 128 $KMeSO_4$, 10 4-(2-hydroxyethyl)-1-piperazineethanesulfonic acid, 1 K_2-ethylene glycol tetraacetic acid (EGTA), 4 $MgCl_2$, 4 Na_2-adenosine triphosphate, 0.4 Na-guanosine triphosphate, 10 Na_2-phosphocreatine, 3 ascorbate; pH 7.3). The intracellular concentration of sodium ion was 28.4 mM, and the calculated reversal potential for sodium was 44.6 mV. In some experiments, biocytin (2–4 mg/mL) was added to the internal solution.

Traces were filtered online with a 10-kHz Bessel filter and digitized (16-bit resolution, USB-6259; National Instruments) with a sampling rate of 40 kHz. One neuron's recordings (performed early in the study) were filtered at 4 kHz and sampled at 10 kHz; these data were excluded from AP waveform analysis but included in firing rate analyses. Experiments were controlled by open-source (www.ephus.org) 'Ephus' software (Suter et al. 2010) on a Microsoft Windows workstation. All the data are reported after subtracting 10.5 mV from the recorded membrane potential to compensate for a calculated liquid junction potential at the interface of pipette and cell interior.

Intrinsic properties were studied by presenting families of current steps ranging in amplitude from −200 to 600 pA in 50 pA increments, with a duration of 1 s, unless indicated otherwise. In each case, the holding potential (V_h) of about −80 mV was maintained by constant current injection. A parallel data set was collected at the resting membrane potential (V_r). Because V_r tended to be close to V_h and because results from the 2 data sets were highly consistent, the data presented are mostly from the V_h data set, except where indicated.

One corticospinal neuron showed strong intrinsic bursting in response to steps of injected current, and was excluded from quantitative analysis; another with bursting only at higher current levels was not excluded. Corticostriatal neurons did not burst, but often displayed an initial doublet at higher current levels; none was excluded from analysis.

"Sag" of the membrane potential was calculated as the percentage difference between the peak amplitude of the initial response (0–0.1 s after step onset) relative to the peak amplitude of the steady-state response (0.9–1.0 s), both measured with respect to the baseline averaged over 0.5 s prior to step onset. We averaged a 5-ms window around the initial and the steady-state peak.

Input resistance was measured from the steady-state responses to a series of hyperpolarizing and subthreshold depolarizing current steps (duration 1.0 s, amplitude ≤ 200 pA), as the slope of a linear least-squares fit to the resulting voltage–current relationship.

Rheobase was estimated as the current-axis intercept of a linear least-squares fit to the frequency–current (f–I) relationship measured from all responses to super-threshold depolarizing current steps (duration 1.0 s).

To quantify the shape of individual AP waveforms, we first identified the threshold (in mV) as the point when dV/dt exceeded 10% of its maximum value, relative to a dV/dt baseline measured 2 ms before the AP peak. The AP peak was taken as the maximum membrane potential reached after threshold, and AP amplitude as the difference between threshold and peak. The AP width was measured at half-amplitude with linear interpolation between samples.

For a statistical comparison of 2 populations where a P-value is reported in the text, we used a 2-sample t-test when both samples were normally distributed (as determined for each by the Lilliefors test), and the Wilcoxon rank-sum test otherwise. For comparison of variance, we used a 2-sample F-test for equal variances when both samples were normally distributed, and the Ansari–Bradley test (after subtracting the medians) otherwise.

Soma Size

A digital image of the soma was captured prior to patching using a ×60 objective lens focused at the depth of the greatest soma cross-section. The soma outline was manually traced (ImageJ, Fiji) and the centroid and maximal cross-sectional area of the resulting closed polygon were calculated with custom software routines. Soma diameter was measured at the greatest horizontal width. We terminated the boundary between the soma and apical dendrite where we discerned the greatest change in taper, similar to previous work (Tseng and Prince 1993). One recorded neuron was excluded from this analysis, as no suitable image was obtained.

Pharmacology

Synaptic blockers were added to the bath solution [2,3-Dioxo-6-nitro-1,2,3,4-tetrahydrobenzo[f]quinoxaline-7-sulfonamide (NBQX) 10 µM,

3-((R)-2-Carboxypiperazin-4-yl)-propyl-1-phosphonic acid (CPP) 5 μM, gabazine 10 μM; Tocris], except where noted.

Channelrhodopsin-2 (ChR2) Photostimulation

Following published methods (Petreanu et al. 2007; Anderson et al. 2010), we transfected cortical progenitor cells at embryonic day 16 by in utero electroporation of ChR2-encoding plasmids, resulting in mice with expression of ChR2 (and Venus fluorescent protein) in a subset of layer 2/3 neurons. In the brain slices prepared in the fourth postnatal week (as described earlier), to stimulate local-circuit inputs to corticospinal neurons, we photostimulated the dendrites and axons of the transfected layer 2/3 neurons by delivering brief light pulses from a blue laser (473 nm, 50 mW; MLL-FN473; CNI Laser), while simultaneously recording postsynaptic responses from a corticospinal neuron (identified by retrograde labeling as described earlier). Photostimulus intensity was set just strong enough so that synaptic inputs induced APs in the postsynaptic neuron.

Laminar Boundaries

To identify laminar boundaries, the brain slices were visualized at low magnification with gradient contrast optics and, digital images of the motor cortex were saved for off-line analysis. Under these imaging conditions, the boundaries between most layers could be readily identified and measurements from many experiments ($n = 60$) were consistent. Normalized to the full thickness of the cortex (pia = 0, white matter = 1), the mean normalized depths of laminar borders (±SD) were layer 1/2, 0.12 ± 0.01; layer 3/5A, 0.32 ± 0.04; and layer 5A/5B, 0.47 ± 0.04. The deeper half of the cortex (layers 5B and 6), however, did not display obvious laminar boundaries. The deeper boundary of layer 5B was defined as the lowermost extent of retrogradely labeled corticospinal somata (normalized depth 0.76 ± 0.04, layer thickness 373 ± 34 μm, mean ± SD, $n = 30$ slices).

Morphological Reconstruction

After recordings were completed, the brain slices containing biocytin-filled neurons were returned to a holding chamber for 1–2 h at room temperature, before fixing in 4% PFA -PB (8% aqueous paraformaldehyde diluted 1:1 with 0.2 M phosphate buffer) for approximately 16 h at 22°C. After fixation, the slices were rinsed thoroughly and maintained in PB, with daily solution changes until further processing. To stain the recorded neurons for 2-photon fluorescence microscopy, the slices were rinsed in Tris-buffered saline (TBS, 7×, 5 min each), permeabilized in TBS–Triton (3%, 1 h), blocked in normal goat serum (NGS, 10%) and bovine serum albumin (BSA, 0.5%) in TBS for 30 min, rinsed in TBS (2×, 5 min each), and stained with streptavidin-Alexa-488 conjugate (1:200; Invitrogen) in TBS with NGS (1%) and BSA (0.5%) for approximately 16 h at 4°C. After staining, the slices were rinsed in TBS (4×, 5 min each) and mounted on a #1 glass cover slip (0.17 mm thickness) in mounting medium (Dako), using additional cover slips as spacers to avoid compression of the tissue. Slides were sealed with nail polish. The samples were shielded from light throughout these procedures.

Fluorescent neurons were imaged on a custom-built 2-photon laser-scanning microscope equipped with a ×25 objective lens (numerical aperture, 0.8; Zeiss), using the lens collar to compensate for differences in index of refraction between the immersion medium (glycerol Type FF; Cargille), cover slip, and mounting medium. The laser was tuned to 810 nm to excite both the dye in the filled neuron and the retrograde tracer for emission in separate channels. Pixels were approximately 0.2–0.5 μm (x and y dimensions), and z steps were 0.84 μm. Image stacks contained up to approximately 1.3 billion voxels, with typically 3–4 stacks required per neuron for the entire dendritic arbor. For visualization, custom software macros (ImageJ, Fiji) automatically flattened the image stacks by maximal intensity z-projection and stitched the resulting tiles starting from stack coordinates recorded during image acquisition, with an automatic optimization step for fine alignment. The stitching step made use of a freely available algorithm (Preibisch et al. 2009). To calibrate the scale of the resulting high-resolution image stacks, epifluorescence images of the live slice and of the fixed slice once mounted were taken with a ×4 objective lens, and the x–y distances between landmarks were compared.

Neuronal morphology was digitally reconstructed using the Neurolucida software (MBF Bioscience). Multiple image stacks were aligned in 3 dimensions, the software was configured for the appropriate voxel size, and the neuron was reconstructed manually. Dendrites were reconstructed as connected trees of tapered cylinders, and the soma as a series of contours. Spines and axon were not reconstructed.

Results

Waveform Properties of Single APs in Corticospinal Neurons at Threshold

Whole-cell recordings in brain slices were targeted to retrogradely labeled corticospinal neurons in the primary motor cortex (Fig. 1A). Corticospinal neurons were all large pyramidal neurons in layer 5B, with "thick-tufted" dendritic morphologies (Fig. 1B). Cell selection was guided solely by (1) the presence of retrograde labeling and (2) the location of the soma in the region corresponding to the forelimb representation area of the somatic motor cortex (Weiler et al. 2008); neither the apparent soma sizes of the cells nor their particular vertical locations within layer 5B (i.e., sublayer location) were used as selection factors. The recorded corticospinal neurons were located across the full range of depths (i.e., vertical positions) within layer 5B (Fig. 1B,C). Soma sizes appeared to vary little across the sample (Fig. 1D). We estimated the size of each recorded neuron's soma by tracing the maximal cross-section of the soma. Soma shape was similar across this population (Fig. 1D), and soma size varied little (mean area: 258 μm$^2 \pm 35$ SD, range 197–325 μm^2, $n = 23$ neurons; mean diameter: 15 μm ± 2 SD, range 12–18 μm; Fig. 1E).

APs were evoked in the recorded neurons by injecting current steps (Fig. 2A). We first analyzed the waveforms of the first AP evoked during a step current injection near firing threshold (Fig. 2B). For consistency, current steps were delivered from a membrane potential of −80 mV, maintained as needed by constant current injection. Resting potentials (V_r; average, −82.7 mV, range −77.7 to −86.6 mV) were close to this value, and key parameters such as AP width were statistically indistinguishable when measured from V_r versus −80 mV. For a sample of 24 corticospinal neurons (from 16 slices and 13 mice), we measured multiple AP-related parameters on the basis of analysis of the recorded membrane potential and dV/dt (Fig. 2C), including AP width, maximum and minimum dV/dt, threshold, peak (maximum depolarization), and amplitude (from threshold to peak; Fig. 2D). Summary statistics for these parameters are given in Table 1. There were no significant correlations between AP waveform and soma area.

Corticospinal APs are Relatively Fast

To compare corticospinal AP properties with those of other cell classes within the same layer in the motor cortex, we recorded from another class of pyramidal neuron, callosally projecting corticostriatal neurons in layer 5B ($n = 10$; located across a range of depths within layer 5B), identified by retrograde labeling. Also, because fast-spiking (FS) interneurons offer a benchmark for "fast" APs, we recorded FS interneurons ($n = 7$; located across a range of depths within layer 5B), identified as fluorescent cells in slices prepared from G42
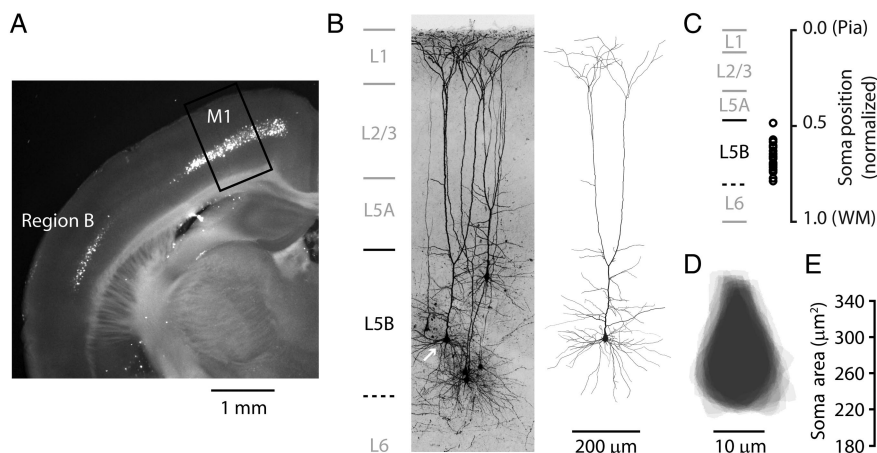
Figure 1. Anatomical location and somatodendritic morphology of retrogradely labeled corticospinal neurons. (*A*) An epifluorescence image of a coronal brain slice prepared several days after injection of a fluorescent tracer into the cervical spinal cord, showing retrogradely labeled corticospinal neurons in layer 5B. Highest densities of labeled somata were found in 2 regions: Primary motor cortex (M1), and a separate lateral area (Region B). Box: Region in M1 where most recordings of M1 corticospinal neurons were made. (*B*) Dye-filled corticospinal neurons identified by retrograde labeling, whole-cell recorded with biocytin in the pipette, and imaged with 2-photon microscopy. Maximum intensity projection of image stacks. Laminar borders (indicated on the left) were measured and averaged from bright-field slice images ($n = 60$). The lower border of layer 5B was estimated from the lower edge of the distribution of bead-labeled corticospinal somata in fluorescence slice images ($n = 30$). Right: Reconstructed morphology of one of the corticospinal neurons (arrow). (*C*) Cortical depths of corticospinal neurons in the main data set plotted as the distance of the soma from the pia, normalized to the cortical thickness (pia to white matter, WM). (*D*) Soma tracings for the recorded corticospinal neurons. Tracings are centroid centered and aligned on the apical axis. (*E*) Cross-sectional areas of the somata (error bars: SD).
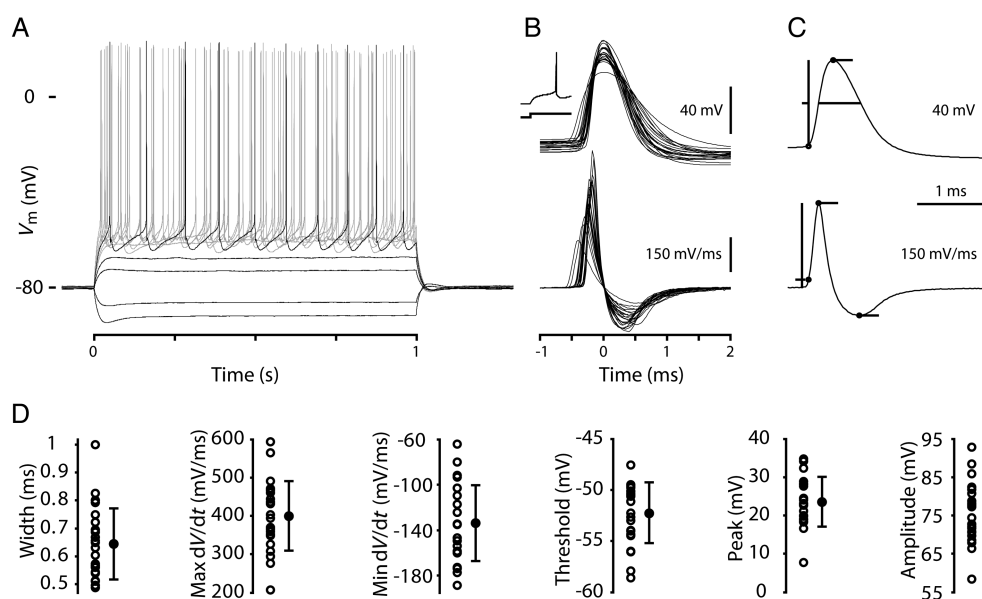

Figure 2. Waveform properties of single APs recorded in retrogradely labeled corticospinal neurons in mouse motor cortex. (*A*) Responses to a family of injected steps of current recorded in a corticospinal neuron. (*B*) Top: Individual AP waveforms from 23 corticospinal neurons overlaid for comparison and peak aligned. Inset shows the first AP during a current step on a longer time base. Bottom: Corresponding dV/dt traces. (*C*) Top: AP example illustrating measurement of waveform parameters. Bottom: Corresponding dV/dt trace indicating the measurement method for time of threshold, maximum rising slope, and minimum falling slope. (*D*) Width, max dV/dt, min dV/dt, threshold, peak, and amplitude measurements for each of the APs shown in (*C*). In addition, each measurement is summarized with error bars indicating 1 standard deviation above and below the population mean.

mice. Furthermore, because of the possibility that corticospinal neurons have faster spikes than some types of interneuron, we also recorded low-threshold-spiking (LTS) interneurons ($n = 9$; located across a range of depths within superficial layer 5B and deep layer 5A), identified as fluorescent cells in slices prepared from GIN mice. The AP width for corticospinal neurons (0.65 ± 0.03 ms; mean ± standard error of the mean [SEM]; $n = 23$) was intermediate compared

with FS interneurons and corticostriatal neurons, and less than for LTS interneurons (Fig. 3*A*,*B*). On average (Fig. 3*C*), APs of corticospinal neurons were significantly longer in duration than those of FS interneurons (by a factor of 2.8; FS: 0.23 ± 0.01 ms; $P < 0.001$, *t*-test), and shorter than those of either corticostriatal neurons (by a factor of 0.6; corticostriatal: 1.04 ± 0.08 ms; $P < 0.001$, *t*-test) or LTS interneurons (by a factor of 0.75; LTS: 0.86 ± 0.02 ms; $P < 0.001$, *t*-test). The short

Table 1

Intrinsic properties of motor cortex corticospinal neurons at 1 month compared with corticostriatal neurons at the same age, and corticospinal neurons recorded at a later age, with a different internal solution, or in a separate cortical area

Parameter	Corticospinal, 1 month	Corticostriatal, 1 month	Corticospinal, 4 months	Corticospinal, no EGTA	Corticospinal, Region B
N	23	10	10	9	7
Resting membrane potential (mV)	-82.7 ± 2.5	-84.3 ± 3.8	-85.4 ± 3.2*	-81.6 ± 4.4	-83.6 ± 3.9
Input resistance (MΩ)	42.7 ± 13.2	90.6 ± 13.4**	35.7 ± 7.6	39.2 ± 12.6	47.1 ± 11.1
Sag (%)	21.0 ± 6.6	6.7 ± 4.8**	20.0 ± 3.6	19.0 ± 6.0	18.5 ± 4.6
AP width (ms)	0.65 ± 0.13	1.04 ± 0.25**	0.51 ± 0.03**	0.59 ± 0.06	0.61 ± 0.03
Maximum dV/dt (mV/ms)	400 ± 91	250 ± 68**	498 ± 55**	492 ± 95*	488 ± 45*
Minimum dV/dt (mV/ms)	-134 ± 33	-66 ± 19**	-175 ± 10**	-153 ± 23	-147 ± 15
AP threshold (mV)	-52.3 ± 3.0	-45.6 ± 3.0**	-55.8 ± 3.0*	-55.4 ± 4.8	-53.7 ± 3.0
AP peak (mV)	23.6 ± 6.5	20.1 ± 5.3**	25.9 ± 3.5	30.2 ± 3.7*	32.2 ± 3.3**
AP amplitude (mV)	75.8 ± 7.9	65.6 ± 6.0**	81.7 ± 3.2*	85.6 ± 6.9**	85.7 ± 4.8**
% change in AP width	0.15 ± 2.9	7.65 ± 5.0**	3.1 ± 3.8*	3.7 ± 4.6*	4.4 ± 5.9*
Estimated rheobase (pA)	341 ± 86	182 ± 73**	361 ± 87	330 ± 76	286 ± 57
f–I slope (Hz/nA)	98 ± 18	61 ± 21**	115 ± 29*	86 ± 24	110 ± 23
f–I linearity index	0.77 ± 0.14	0.61 ± 0.10**	0.75 ± 0.18	0.82 ± 0.26	0.80 ± 0.17
SFA ratio	0.87 ± 0.24	1.70 ± 0.25**	0.88 ± 0.20	1.03 ± 0.34	0.77 ± 0.11

Values represent the sample mean $\pm$ SD. The % change in AP width is based on comparison of the first to eighth APs at 10 Hz. The f–I linearity index is defined below (Fig. 8H). Spike frequency adaptation (SFA) ratio: Average of the last 2 ISIs divided by the average of the first 2 ISIs. Reported P-values are by t-test, except for AP threshold, where Wilcoxon rank-sum test was used. P-values are based on comparison of each data set with the 1-month corticospinal data set.
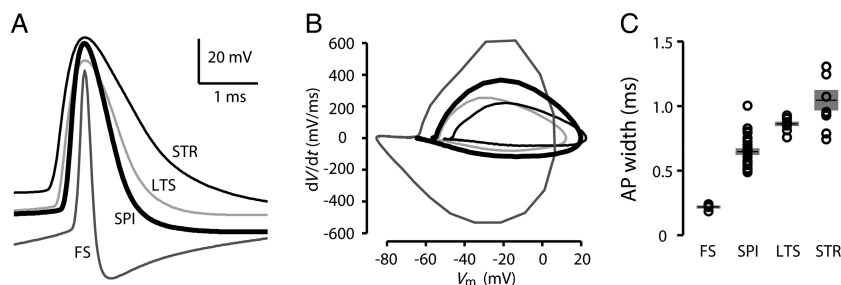*$P < 0.05$, **$P < 0.005$.

Figure 3. Width of APs evoked by current steps in corticospinal neurons compared with other cell types. (*A*) Example AP waveforms from a corticospinal neuron (SPI), corticostriatal neuron (STR), FS interneuron (FS), and LTS interneuron (LTS). (*B*) Phase plots of same APs shown in (*A*). (*C*) Plot of AP width, group data. Bars: mean $\pm$ SEM.

duration of corticospinal APs was associated with a low AP threshold (on average 6.7 mV lower than for corticostriatal neurons), with no significant difference in AP peak depolarization.

Synaptic Excitation Evokes Even Faster APs Compared with Somatic Current Injection

Step current injection delivered via a patch pipette at the soma is a convenient standard approach for evoking APs and characterizing their waveform properties, but APs elicited this way could potentially differ from APs resulting from synaptic depolarization. To explore this, we used an optogenetic paradigm for transfecting layer 2/3 pyramidal neurons with ChR2 (Petreanu et al. 2007), enabling photostimulation of (presynaptic) layer 2/3 pyramidal neurons and their axons while recording from a (postsynaptic) retrogradely labeled corticospinal neuron in the slice (holding V_m at -80 mV with current injection as needed). Stimulus intensity was set so that photo-evoked synaptic inputs were just strong enough that the compound excitatory postsynaptic potential generated an AP in the postsynaptic corticospinal neuron (Fig. 4A, inset). Application of synaptic blockers (NBQX 10 μM, CPP 5 μM, gabazine 10 μM) showed that the responses depended on synaptic stimulation (Fig. 4A). APs evoked by synaptic stimulation were 17% faster than those evoked by somatic current steps (duration: 1 s; $P = 0.0012$, paired t-test; $n = 4$ neurons; Fig. 4A,

B), and nearly equal to those evoked by brief somatic current pulses (duration: 10 ms; $P = 0.13$, paired t-test). This analysis indicated that the waveforms of APs evoked either by somatic current steps or by synaptic input appeared broadly similar; however, the use of prolonged current injection to induce APs may slightly overestimate the duration of synaptically driven APs.

Consistent with this conclusion, the waveforms of rare, spontaneous APs closely resembled APs evoked by somatic current injection. Spontaneous APs (observed in 5 of 70 corticospinal neurons, despite the presence of synaptic blockers) rose sharply from a resting potential of around –80 mV, suggesting a distant initiation site. Spontaneous APs occur in interneurons (Sheffield et al. 2011), but are rarely observed in neocortical pyramidal neurons. In each case, the corticospinal neuron exhibited otherwise typical intrinsic properties. Spontaneous APs closely matched those evoked by somatic current injection: Brief, large-amplitude somatic stimulation resulted—apart from a shift in threshold—in waveforms indistinguishable from spontaneous APs, while APs evoked by prolonged somatic stimulation exhibited identical rising phases, but slightly increased duration (Fig. 4C).

AP Waveform During Repetitive Firing

To evaluate AP waveforms during repetitive firing, the current step amplitude was increased to evoke APs at about 10 Hz
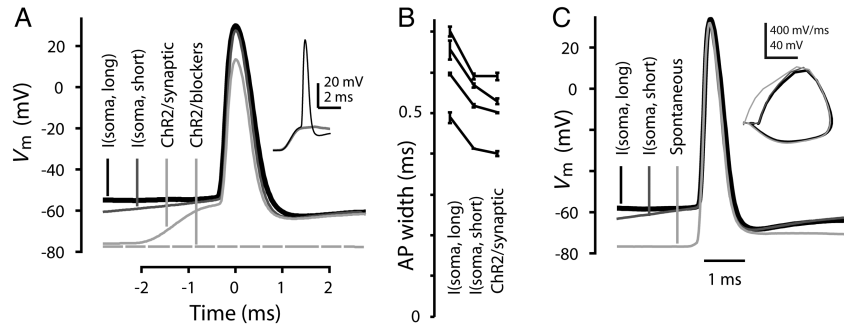
Figure 4. Width of APs evoked by current steps in corticospinal neurons compared with synaptically evoked and spontaneous APs. (*A*) Peak-aligned waveforms of APs evoked in a corticospinal neuron either by current steps injected via the somatic patch electrode (I(soma, short) and I(soma, long): 800 pA, 10 ms or 500 pA, 1 s current steps, respectively), or by photoexcitation of ChR2 expressing layer 2/3 pyramidal neurons (ChR2/synaptic). The lowermost trace shows the absence of photo-evoked response after application of 10 μM NBQX, 5 μM CPP, and 10 μM gabazine to block synaptic transmission. Inset: As shown by these subthreshold (gray) and suprathreshold (black) traces, stimulation intensity was near AP threshold (scale: 20 mV, 2 ms). (*B*) Widths of APs induced by long or short somatic current steps or by synaptic excitation (*n* = 4 neurons), plotted as mean ± SD, averaged over multiple stimulations (range: 2–7) per neuron. (*C*) Spontaneously occurring AP waveform compared with APs evoked by brief or prolonged somatic current injection in a corticospinal neuron (animal age P49). Inset: Phase-space representation of the APs.
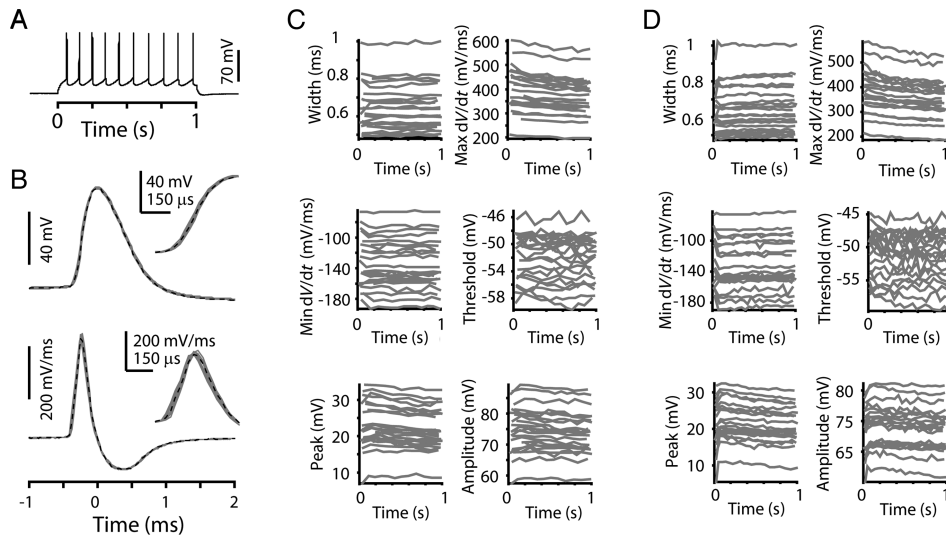

Figure 5. AP width and other waveform parameters remain constant during repetitive firing in corticospinal neurons. (*A*) A train of 10 APs from a corticospinal neuron held near −80 mV with a 100 pA constant current injection, in response to a 300 pA, 1-s current step. (*B*) Upper: Individual AP waveforms from the train in *A* aligned to time of peak membrane potential; the first AP is in black (dashed line) and all subsequent APs in gray. Inset: Rising edge of APs shown with slower time base. Lower: Corresponding d*V*/d*t* traces as in upper panel. Inset: d*V*/d*t* traces of rising edge of AP. (*C*) Multiple AP waveform parameters for 10 Hz trains in individual corticospinal neurons. Same group of 23 corticospinal neurons as in Figure 1. (*D*) Same as (*C*), but for 20 Hz trains.

(Fig. 5*A*), similar to in vivo firing rates reported for layer 5 neurons in the motor cortex in rats (Isomura et al. 2009) and rabbits (Beloozerova et al. 2003). AP waveforms and corresponding d*V*/d*t* traces from the 10 Hz example in Figure 5*A* are aligned to peak time and overlaid for comparison in Figure 5*B*. Even with increased time resolution, the rising edge of the first (black dashed trace) and subsequent (gray traces) APs were nearly identical (Fig. 5*B*). Quantification of AP parameters as a function of AP number in a 10-Hz train showed that individual neurons all maintain consistent AP waveforms during repetitive firing (Fig. 5*C*). Repeating this analysis for 20 Hz trains showed a similar pattern of AP waveform stability over time (Fig. 5*D*).

Corticospinal–Corticostriatal Comparison of AP Properties During Repetitive Firing

In contrast to the steady AP waveforms of corticospinal neurons during repetitive firing, corticostriatal AP waveforms

broadened significantly more during current steps (Fig. 6). The broadening occurred from the first to the second AP, with subsequent AP waveforms remaining relatively stable and nearly as wide as the second AP (Fig. 6*B*,*C*). The change in waveform between the first and the eighth APs was approximately 8% on average (Fig. 6*D*; 10% for the second AP, 7% for the subsequent APs) and was associated with a slowing of the falling edge (minimum d*V*/d*t*; Fig. 6*E*).

AP Waveform Variability: Within-Cell Versus Across-Cell Analysis

A qualitative impression that emerges from the foregoing analyses of AP waveform properties of corticospinal neurons is that the within-cell variance appears substantially lower than the variance across different cells in the population. To quantify this, we calculated the coefficient of variation (CV) for AP waveform properties within cells (i.e., based on the parameter values for the approximately 10 APs in a train) and also
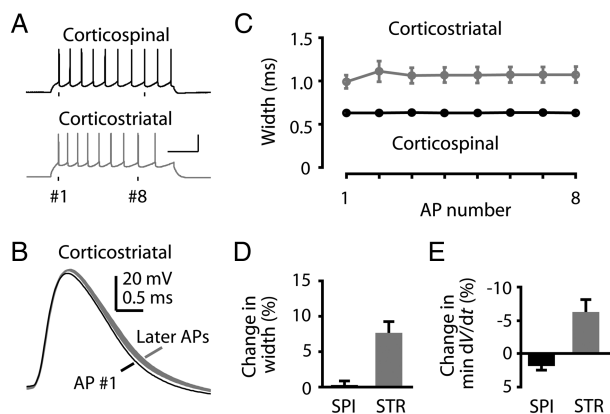
Figure 6. AP waveform constancy during repetitive firing: Comparison of corticospinal and corticostriatal neurons. (*A*) Example trains of APs at approximately 10 Hz in corticospinal and corticostriatal neurons. (*B*) Individual corticostriatal AP waveforms from a 10-Hz train. Black: first AP; gray: Subsequent APs. (*C*) Width of successive APs in a 10-Hz train averaged for corticospinal (black, *n* = 23) and corticostriatal (gray, *n* = 10) neurons (mean ± SEM). (*D*) Percent difference from first to eighth AP for the change in AP width. (*E*) Percent difference from first to eighth AP for the change in falling slope (minimum d*V*/d*t*).
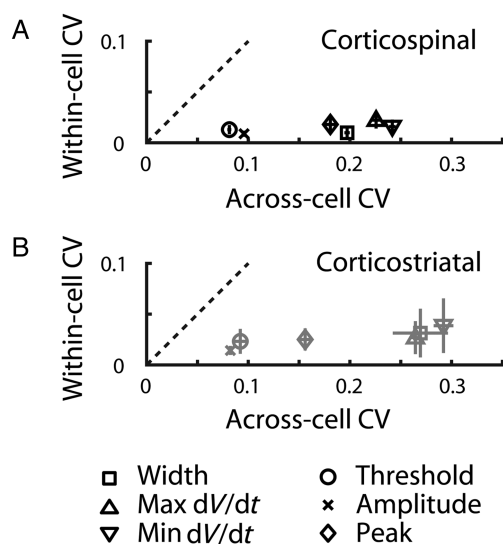

Figure 7. Individual corticospinal neurons maintain consistent AP shape. (*A*) AP waveform variability across the corticospinal population is greater than variability within APs from an individual neuron. For each neuron, the within-cell CV was calculated for the AP waveform properties across the approximately 10 APs in an approximately 10-Hz train evoked by a depolarizing current step. For each neuron, the average values of these properties were also determined, and the CV of these average values was calculated across the sample of neurons to obtain the across-cell CV. Error bars represent the SEM. Dashed lines: Unity slope. (*B*) Same analysis for corticostriatal neurons.

across cells (i.e., based on the average parameter values for each cell), for trains of APs at approximately 10 Hz. The plot of the within-cell CV versus the across-cell CV confirmed that the former was indeed much smaller for all waveform properties (Fig. 7*A*). For example, the CV of corticospinal AP widths was only 0.0098. A similar pattern was observed for corticostriatal neurons (Fig. 7*B*).

Repetitive Firing: Frequency–Current (f–I) Relationships

To characterize the intrinsic excitability of corticospinal neurons, we calculated *f–I* relationships from their responses to families of current steps (Fig. 8*A,B*). These were similar after baseline subtraction of the holding current required to maintain the membrane potential at a baseline of −80 mV prior to steps, and also when responses were obtained at the resting membrane potential (data not shown). The 2 curves representing the average *f–I* relationships measured either from −80 mV or from the resting membrane potentials (−82.7 ± 2.5 mV, mean ± SD, range: −77.7 to −86.6 mV; *n* = 23) appeared shifted by approximately 50 pA (Fig. 8*C*), in agreement with the value of approximately 60 pA predicted (from Ohm's law) by the average resting membrane potential and input resistance (42.7 ± 13.2 MΩ, mean ± SD, *n* = 23). In contrast, *f–I* relationships for individual corticostriatal neurons (Fig. 8*D*) were notable for shallower slopes and more pronounced "rollover" (i.e., sublinearity; progressively less increase in firing rates with increasing current injection). Thus, the form of the average (threshold-adjusted) *f–I* relationship differed for the 2 cell types (Fig. 8*E*), with corticospinal neurons exhibiting steeper *f–I* slopes (Fig. 8*F*), higher rheobases (Fig. 8*G*), and greater *f–I* linearity (Fig. 8*H*) compared with corticostriatal neurons (Table 1). The slopes of *f–I* relationships of corticospinal neurons averaged approximately 100 Hz/nA (Fig. 8*F*). Within the corticospinal sample, there was only a weak positive correlation ($R^2 = 0.16$, $P = 0.001$) between *f–I* slope and input resistance, but a strong negative correlation ($R^2 = 0.58$, $P = 1.2\mathrm{e}{-13}$) between rheobase and input resistance (Fig. 8*I*), suggesting that above the firing threshold the gain is primarily influenced by active membrane properties.

To explore the upper limit of high-frequency firing in corticospinal neurons, we recorded at the soma ($n = 4$) while electrically stimulating the descending axon in the subjacent white matter (10-pulse trains at varying frequencies). Corticospinal neurons faithfully followed frequencies as high as 450 Hz, exceeding 300 Hz in all cases.

Repetitive Firing: Lack of Spike Frequency Adaptation

The firing rates of corticospinal neurons appeared stable over the time course of current steps, in some cases adapting slightly and in other cases accelerating (Fig. 9*A*) similar to previous observations of pyramidal tract-type pyramidal neurons in the motor cortex (Miller et al. 2008). The examples (Fig. 9*A*) show typical firing patterns of representative corticospinal neurons (selected for similar steady-state firing rates, with the last interspike interval (ISI) ranging from 74 to 77 ms). The plot of the instantaneous firing rate as a function of time showed that corticospinal neurons consistently maintained stable firing (Fig. 9*B,C*). Corticostriatal neurons, in contrast, and in accordance with prior studies (Hattox and Nelson 2007), showed strong spike frequency adaptation (Fig. 6*A*, and 9*C*), with spike frequency adaptation ratios (defined as the average of the last 2 ISIs divided by the average of the first 2 ISIs during a ~10-Hz train) always greater than unity (1.70 ± 0.25, mean ± SD, *n* = 10) and on average 2-fold greater than in corticospinal neurons (0.87 ± 0.24, mean ± SD, *n* = 23).

Confirmation of the Main Findings with a Different Internal Solution

The internal solution used in this study contained the calcium chelator EGTA (1 mM). Earlier studies in the cat have described calcium-dependent potassium currents in large layer 5
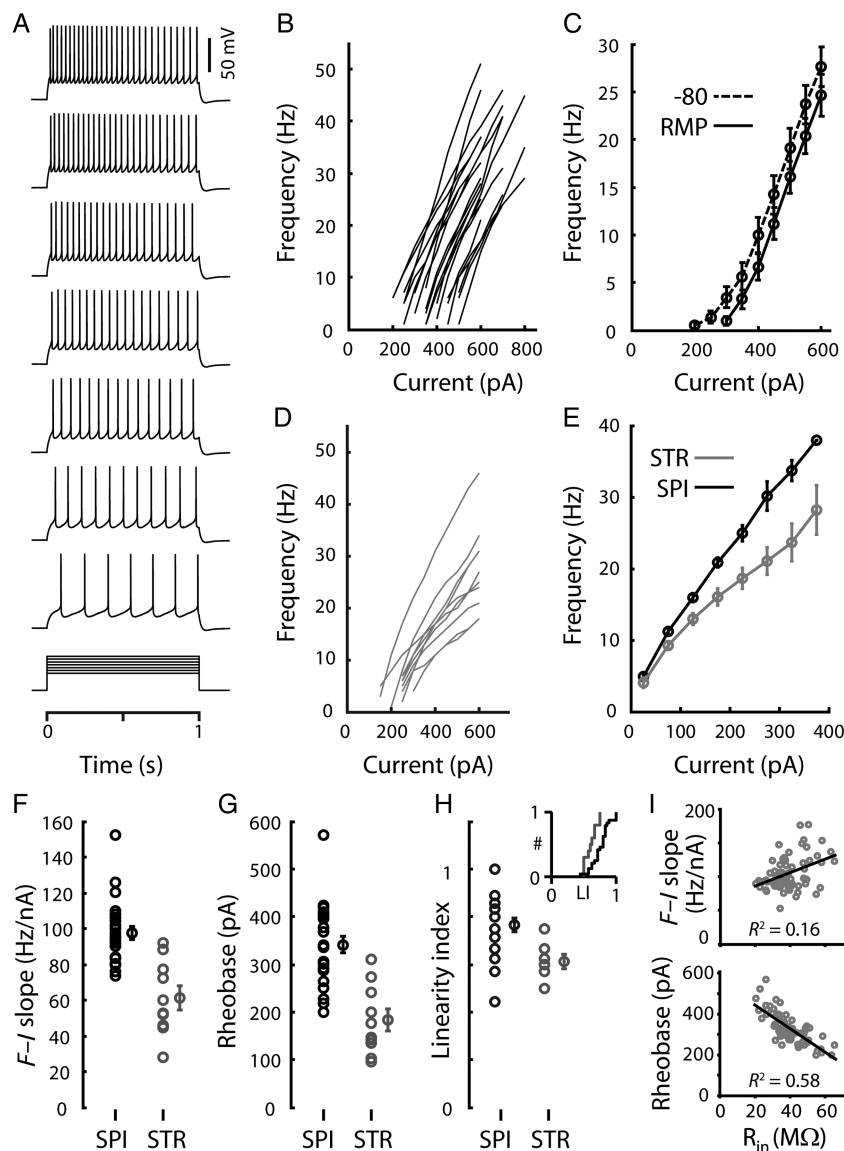
Figure 8. Corticospinal frequency–current (*f–I*) relationships. (*A*) A corticospinal neuron's suprathreshold responses to a family of current steps (300–600 pA) delivered from rest. (*B*) Corticospinal neurons' *f–I* relationships measured from a holding potential of −80 mV. (*C*) Average *f–I* relationships of corticospinal neurons measured at −80 mV (dashed line) or at the resting membrane potential (solid line). (*D*) *f–I* relationships of 10 individual corticostriatal neurons measured from a holding potential of −80 mV. (*E*) Average *f–I* relationships of corticostriatal (dashed line) and corticospinal (solid line) neurons measured from the resting membrane potential. Current values represent the amplitudes of the step stimuli minus the amplitude of the first AP-evoking step; the values were binned prior to averaging. (*F*) *f–I* slopes (left, individual values; right, mean ± SEM). (*G*) Estimated rheobase (left, individual values; right, mean ± SEM). (*H*) Linearity index (LI; left, individual values; right, mean ± SEM). Because many of the data points overlap, the cumulative distributions are also shown (inset). LI was calculated as the ratio of the *f–I* slope for large versus small current steps: LI = (slope over the third interval)/(slope over the first interval). Thus, LI = 1 would indicate perfect linearity (constant slope), and LI = 0 would indicate complete rollover (reduced slope). (*I*) Relationships between *f–I* slope and input resistance (R_{in}) (top) and between estimated rheobase and R_{in} (bottom). All corticospinal neurons in the study were included in these analyses. Lines represent linear regressions.

pyramidal neurons, primarily affecting slow afterhyperpolarizations (Schwindt et al. 1988). EGTA could thus potentially reduce spike frequency adaptation and modify the *f–I* curve (e.g. shift toward lower rheobase, or increase in linearity or gain). We, therefore, performed additional recordings without EGTA in the intracellular solution. Compared with the corticospinal neurons recorded with our standard conditions, the EGTA-free properties were mostly identical, including AP width, *f–I* relationship, and spike frequency adaptation (Table 1). Because a calcium chelator might affect the regularity of AP timing, we calculated the CV across ISIs in approximately 10 Hz trains; however, the CV_{ISI} were not

significantly different ($P = 0.71$) with (0.29 ± 0.02, mean ± SD, $n = 23$) or without EGTA (0.29 ± 0.03, mean ± SD, $n = 9$). Thus, EGTA minimally affected the intrinsic properties of corticospinal neurons examined here.

Older Animals Exhibit Similar Corticospinal Properties

The preceding data were collected from approximately 1-month-old mice. To assess the age-dependence of corticospinal AP properties, we recorded corticospinal neurons from mice up to 4 months of age ($n = 6$ at P42, $n = 6$ at P49, $n = 6$ at 11 weeks, $n = 10$ at 16 weeks). Retrograde labeling was always performed a few days prior to experiments. The areal
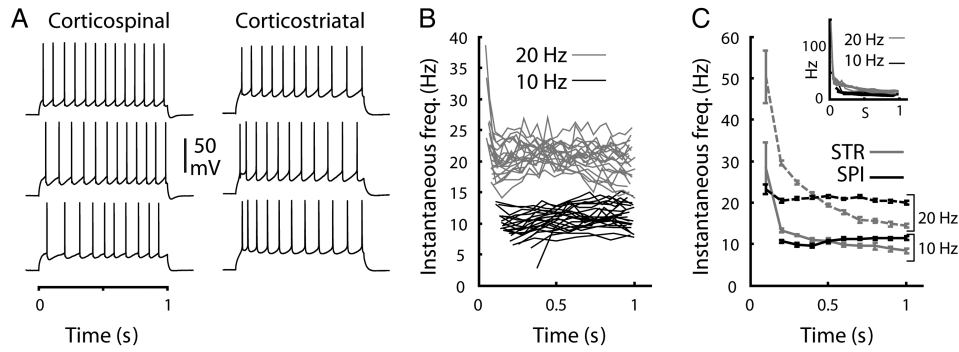
Figure 9. Spike frequency over time. (*A*) Example trains of APs at approximately 10 Hz in corticospinal (left) and corticostriatal neurons (right), showing the range of spike-frequency modulation over time. Examples were selected on the basis of similar steady-state firing rate (last ISI ranges from 74 to 77 ms for corticospinal, 113–119 ms for corticostriatal). (*B*) Instantaneous firing rate as a function of time from the onset of the current step for traces with approximately 10 (bottom traces, black lines) or 20 Hz (top traces, gray lines) average firing rates. (*C*) Instantaneous firing rate versus time averaged for all 10 (bottom, solid lines) or 20 Hz (top, dashed lines) traces, for corticospinal (black lines) and corticostriatal (gray lines) neurons. Inset: Data for individual corticostriatal neurons.
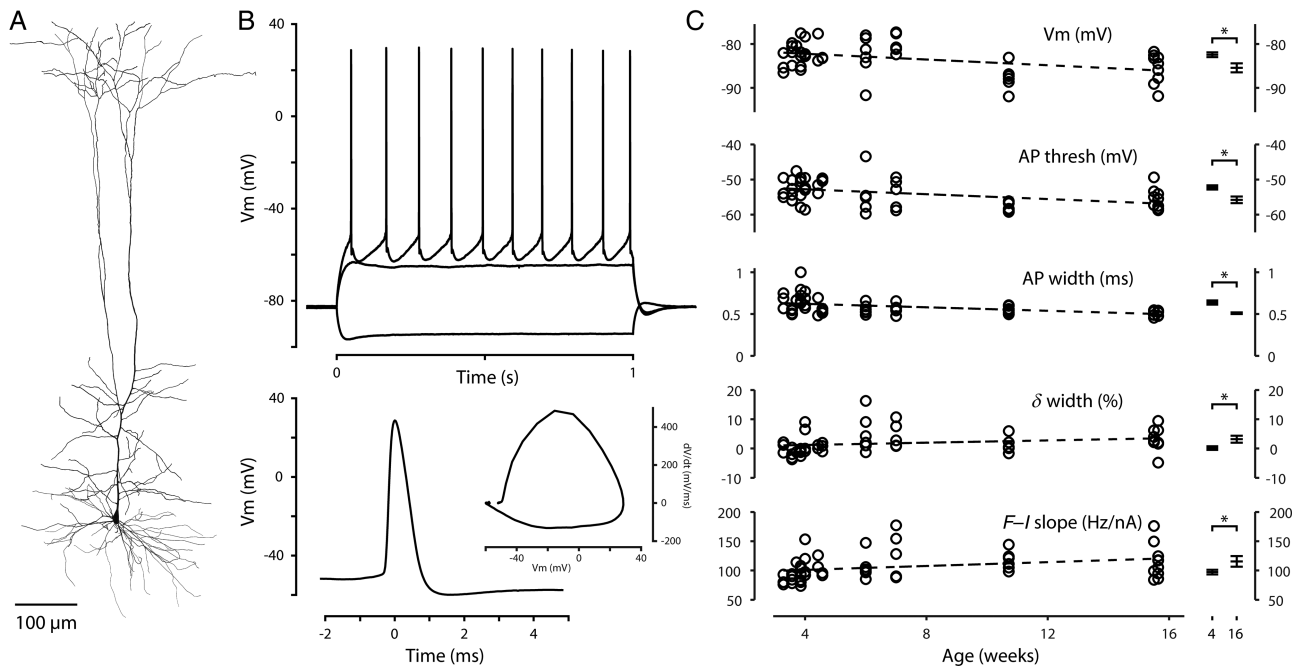

Figure 10. Corticospinal intrinsic properties of older animals. (*A*) Reconstructed morphology of a corticospinal neuron from an older mouse (age P49). (*B*) Top: Responses to a family of injected steps of current (−300, +300, and +400 pA) recorded in the corticospinal neuron shown in (*A*). Bottom: Waveform of the first AP in the train shown at top. Inset: Phase-space representation of the same AP. (*C*) Intrinsic properties that varied with animal age. Each data point represents a single corticospinal neuron; the dashed line represents a linear fit to the data. The asterisk indicates a statistically significant ($P < 0.05$) difference between neurons from the original data set (∼4 weeks of age) and from the oldest animals (∼16 weeks of age). A few additional AP parameters differed between these age groups (see text). The δ width parameter is the change in AP width at approximately 10 Hz (percent difference from first to eighth AP).

distribution of bead-labeled neurons and their morphology (Fig. 10*A*) appeared no different in older animals. We selected 14 intrinsic properties for quantification (Table 1) and calculated linear regressions to age. Most parameters showed no significant correlation (zero slope fell within the 95% confidence intervals); however, a small but significant trend was found toward taller, narrower APs and a more negative resting potential (Fig. 10*B,C*), similar to the trends reported over the first 7 weeks for rat thick-tufted layer 5 neurons (Kasper et al. 1994). Comparison of APs from the oldest animals (∼4 months) with those reported earlier for young adults (∼1 month) showed that on average the AP threshold

dropped by 3.5 mV, and the width was 79%, accompanied by an increase in the maximal rates of rise (25%) and fall (31%). Resting membrane potential dropped by approximately 3 mV, while input resistance, voltage sag, subthreshold resonance (Sheets et al. 2011), and rheobase were unchanged. Repetitive firing properties also remained similar, though the slope of the *f–I* relationship was about 17% greater in older animals. As above, we quantified the change in AP width during approximately 10 Hz trains and found a small (∼3%) increase in width from the first to the eighth AP, compared with the first AP near threshold. AP width appeared remarkably consistent in the oldest animals (Fig. 10*C*); comparison of the
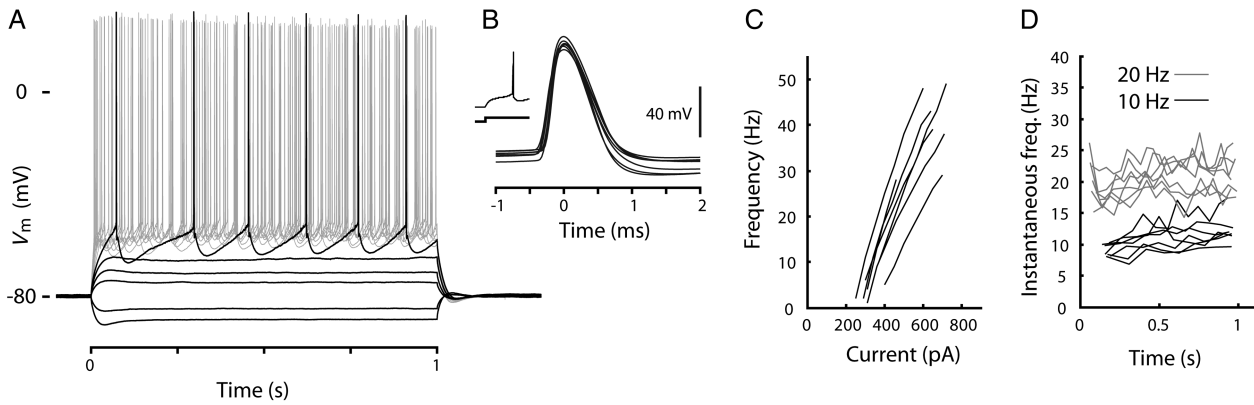
Figure 11. Intrinsic properties of corticospinal neurons in Region B. (*A*) Traces recorded from a corticospinal neuron in Region B. (*B*) AP waveforms; each trace is from a different neuron. (*C*) *f*–*I* relationships. (*D*) Instantaneous frequency over time for traces with approximately 10 and 20 Hz average firing rates.

variance across both groups revealed reduced variability with age for AP width ($P = 0.0003$), and also for the maximal rate of fall ($P = 0.001$) and amplitude ($P = 0.009$); the variance was not significantly different for the other parameters. We conclude that the characteristic intrinsic properties of corticospinal neurons are nearly mature in month-old animals and continue to show small changes beyond this time point.

Corticospinal Neurons in a Separate Cortical Area Have Similar Intrinsic Properties

Because all the preceding recordings were performed in a single cortical area corresponding to the forelimb representation of the primary motor cortex, we wondered whether corticospinal neurons in a separate cortical area possess similar properties. In mammals, in addition to the main population of corticospinal neurons in the primary motor (and sensorimotor) cortex, a secondary population of corticospinal neurons is located on the dorsolateral aspect of the cortex in an area corresponding to the secondary somatosensory cortex, also termed "Region B" (Nudo and Masterton 1990; Fig. 1*A*). For a sample of 7 Region B corticospinal neurons, the intrinsic properties closely resembled those of primary motor cortex corticospinal neurons (Fig. 11; Table 1). While AP width and threshold were not significantly different, APs in the lateral population reached a higher peak depolarization on average (32.2 ± 3.3 mV, mean $\pm$ SD) with a greater maximal rising slope (488 ± 45 mV/ms, mean $\pm$ SD). We also observed a small (4%) increase in AP width in approximately 10 Hz trains. Both populations showed similar sag in response to hyperpolarizing current steps, and despite their slightly smaller size (mean area: $220 \, \mu m^2 \pm 51$ SD, range 155–293 μm^2), input resistance was not significantly different (47 ± 11 MΩ, mean $\pm$ SD) from that in the primary motor cortex. Repetitive firing properties (spike-frequency adaption, estimated rheobase, *f*–*I* slope, and *f*–*I* linearity index) were very similar in both cortical areas.

Discussion

Recording from corticospinal neurons in brain slices of mouse motor cortex, we characterized key suprathreshold aspects of the intrinsic electrophysiological properties of this important class of neocortical pyramidal neurons. These data indicate a triad of spike-related properties characteristic of corticospinal

neurons, compared with another class of pyramidal neurons in motor cortex, corticostriatal neurons: 1) APs were fast, essentially independent of firing rate; 2) firing rates were steady over time, that is, corticospinal neurons had non-adapting firing patterns; 3) firing rates increased in direct proportion to injected current, that is, corticospinal neurons had relatively linear, steep *f*–*I* relationships.

Regarding spike widths, corticospinal APs were approximately 60% as wide as corticostriatal APs and approximately 75% as wide as LTS interneuron APs; however, they did not approach the speed of APs of FS interneurons, which were faster by a factor of approximately 3 on average. The AP waveform parameters related to the fast APs of corticospinal neurons (e.g. width, maximum and minimum d*V*/d*t*) remained constant during repetitive firing at 10 and 20 Hz. The constancy of corticospinal AP waveform parameters during repetitive firing suggests a high safety factor for AP generation (Madeja 2000); alternatively, or in addition, other AP repolarization mechanisms (e.g. Kv3 channels) could contribute to maintaining the fast AP waveform during sustained depolarization and repetitive firing (Rudy and McBain 2001). It also argues against the participation of calcium-dependent potassium currents in AP repolarization (Spain et al. 1991b).

Subtypes of neocortical pyramidal neurons with fast APs have been noted in a variety of previous studies, including 1) pyramidal tract-type neurons identified by antidromic activation (Stefanis and Jasper 1964; Takahashi 1965; Calvin and Sypert 1976; Dykes et al. 1988); 2) electrophysiologically classified pyramidal neurons (Spain et al. 1991a; Chen et al. 1996b; Nowak et al. 2003; Chen and Fetz 2005); 3) morphologically classified pyramidal neurons (Mason and Larkman 1990); and 4) projection neurons identified by retrograde labeling (Tseng and Prince 1993; Kasper et al. 1994; Christophe et al. 2005; Hattox and Nelson 2007; Le Bé et al. 2007; Dembrow et al. 2010). Our results show that fast APs are also a property of corticospinal neurons in mouse motor cortex.

Why fast APs might be advantageous for corticospinal neurons is unclear, but may relate to their distinct anatomy, their unique roles in motor physiology, or both. For example, faster APs could limit calcium influx during prolonged AP trains, reducing activation of potassium channels responsible for spike-frequency adaptation and thus favoring a more regular firing pattern; this in turn could facilitate rate-coded output to the spinal cord. That fast somatic APs are indeed associated with fast axonal APs is indicated by the correlation

between somatically recorded AP width and axonal conduction velocity for pyramidal tract-type projection neurons in cat and primate cortex (Stefanis and Jasper 1964; Takahashi 1965; Naito et al. 1969; Calvin and Sypert 1976; Deschenes et al. 1979; Murray and Coulter 1981; Sakai and Woody 1988; Baranyi et al. 1993; Rathelot and Strick 2006; Vigneswaran et al. 2011).

The spike-to-spike waveform constancy of the APs of individual corticospinal neurons stood in contrast to the greater heterogeneity of waveform parameters across the sample of different corticospinal neurons recorded here, as illustrated by the much lower within-cell than across-cell CV in the parameter values. This variability is broadly consistent with the heterogeneity previously observed in various intrinsic properties of rat corticospinal neurons (Tseng and Prince 1993).

Regarding the repetitive firing properties of corticospinal neurons, the *f–I* relationships of corticospinal neurons were notable for their linearity. The linearity was readily appreciated in the *f–I* relationships of individual neurons (Fig. 8*B*) and in the average *f–I* relationship when the currents were normalized to the threshold current level (Fig. 8*E*). Averaging *f–I* relationships without this normalization (Fig. 8*C*) showed a more sigmoidal curve, reflecting the aggregate behavior of a diverse population of corticospinal neurons in the motor cortex. The linearity seen at the level of individual neurons is at least partly explained by the ability of corticospinal neurons to sustain a constant firing rate over the duration of step current injections (Fig. 9), that is, corticospinal neurons were non-adapting and in some cases even accelerating, as previously described for other pyramidal tract-type projection neurons (Calvin and Sypert 1976; Mason and Larkman 1990; Tseng and Prince 1993; Morishima and Kawaguchi 2006; Hattox and Nelson 2007; Miller et al. 2008; Dembrow et al. 2010). One interpretation of the linearity of corticospinal *f–I* relationships is that corticospinal neurons are efficient at rate-coding (similar to spinal motor neurons). In addition to being linear, corticospinal *f–I* relationships were also relatively steep, a property also previously reported for other types of pyramidal tract-type neurons (Hattox and Nelson 2007). This steepness implies a high gain in transforming synaptic input into spiking output and could, in principle, be a factor underlying the high firing rates observed among layer 5 neurons in motor cortex in vivo (Chen and Fetz 2005; Isomura et al. 2009).

Corticospinal soma size was not associated with AP waveform variability. In other species, certain electrophysiological properties, such as axonal conduction velocity (Naito et al. 1969; Deschenes et al. 1979) and repetitive firing pattern (Tseng and Prince 1993), do correlate with somatic size. The restricted range of soma sizes observed here for mouse corticospinal neurons may have been a factor. In non-rodent species, the distributions of both corticospinal soma size and AP properties are broader (Stefanis and Jasper 1964; Takahashi 1965; Naito et al. 1969; Calvin and Sypert 1976; Deschenes et al. 1979; Murray and Coulter 1981; Sakai and Woody 1988; Baranyi et al. 1993; Rathelot and Strick 2006; Vigneswaran et al. 2011). Furthermore, corticospinal somata are small in mice, similar to other small rodents such as voles and shrews but smaller compared with larger rodents and many other mammalian species such as carnivores and primates (Nudo et al. 1995), consistent with the smaller size of mice, their slightly thinner neocortex, and the smaller size of their

cortical pyramidal neurons (Schuz and Palm 1989; Braitenberg and Schuz 1998). Interestingly, corticospinal tract volleys measured in the spinal cords of mice are notable both for slow conduction velocities (Alstermark and Ogawa 2004; Tanaka et al. 2004) and for sustained synchronization during propagation down the cervical cord, indicating a relatively homogeneous distribution of corticospinal axon diameters (Alstermark and Ogawa 2004); these properties are consistent with our observations of relatively small and homogeneous soma sizes of corticospinal neurons in mouse motor cortex. Thus, both electrophysiology and morphology of corticospinal neurons in the mouse appear to be less heterogeneous than in many other mammals.

Interestingly, while the properties of corticospinal neurons differed from those of corticostriatal neurons, they, in many respects, resemble those of excitatory neurons in the brainstem motor system. In particular, neurons located in a wide variety pre-cerebellar nuclei, receiving highly diverse inputs but all projecting mossy fibers to the cerebellum, uniformly exhibit fast APs, relatively non-adapting repetitive firing, linear *f–I* relationships, and voltage sag due to I_h (Kolkman et al. 2011). Corticospinal neurons also project to neurons in the pontine nuclei (which are pre-cerebellar); thus, our analysis demonstrates that an important class of pre-pre-cerebellar neurons in the motor system shares these properties as well. We speculate that other types of (non-corticospinal) cortico-pontine neurons in other neocortical areas are likely to exhibit these properties as well.

Our findings are likely to have important implications for waveform analysis of spikes recorded in vivo from neurons in the motor cortex. In particular, a recent study demonstrated that for a subset of pyramidal tract projecting neurons recorded in primate motor cortex, presumed to be corticospinal neurons (Betz cells), APs were remarkably fast, with AP widths in the range expected for interneurons (Vigneswaran et al. 2011). Here, in mouse motor cortex, we found that APs of corticospinal neurons were faster than for corticostriatal pyramidal neurons and LTS interneurons, but slower than for one major class of interneurons, FS interneurons. Thus, our findings both corroborate the primate findings, showing that corticospinal neurons have APs even faster than some interneurons, and contrast with them, showing that in the mouse the widths of APs are distinguishable from at least one major class of interneurons. However, APs of many non-FS interneurons are generally slower (Wang et al. 2004), in a range that would overlap with mouse corticospinal neurons. This overlap implies hazard for identifying cell types on the basis of AP waveform alone. Extracellular recordings of in vivo spiking activity are often analyzed on the basis of spike width to sort cells into classes representing putative interneurons and pyramidal neurons. Our findings suggest that while this may suffice (at least in the mouse) for distinguishing FS interneurons from other classes, additional measures may be required for further identification of different classes of inhibitory and excitatory neurons within the large group of non-FS neurons. In layer 5 of mouse neocortex, at least half of the interneurons are non-FS-type (Rudy et al. 2011). Accurate identification of cell types will be particularly important for in vivo assessment of microcircuit connectivity (e.g. based on relative spike timing in multiunit recordings). In the case of rodent motor cortex, corticospinal neurons receive inhibitory input from both FS and LTS interneurons (Tanaka et al. 2011;

Apicella et al. 2012) in addition to excitatory input both from other corticospinal neurons and from other classes of pyramidal neurons (Anderson et al. 2010; Kiritani et al. 2012), and these classes are likely to be differentially active in different behavioral modes.

Funding

Notes

References

Akintunde A, Buxton DF. 1992. Differential sites of origin and collateralization of corticospinal neurons in the rat: a multiple fluorescent retrograde tracer study. Brain Res. 575:86–92.

Alstermark B, Ogawa J. 2004. In vivo recordings of bulbospinal excitation in adult mouse forelimb motoneurons. J Neurophysiol. 92:1958–1962.

Anderson CT, Sheets PL, Kiritani T, Shepherd GMG. 2010. Sublayer-specific microcircuits of corticospinal and corticostriatal neurons in motor cortex. Nat Neurosci. 13:739–744.

Apicella A, Wickersham IR, Seung HS, Shepherd GMG. 2012. Laminarly orthogonal excitation of fast spiking and low threshold spiking interneurons in mouse motor cortex. J Neurosci. 32:7021–7033.

Ayling OG, Harrison TC, Boyd JD, Goroshkov A, Murphy TH. 2009. Automated light-based mapping of motor cortex by photoactivation of channelrhodopsin-2 transgenic mice. Nat Methods. 6:219–224.

Baranyi A, Szente MB, Woody CD. 1993. Electrophysiological characterization of different types of neurons recorded in vivo in the motor cortex of the cat. II. Membrane parameters, action potentials, current-induced voltage responses and electrotonic structures. J Neurophysiol. 69:1865–1879.

Beloozerova IN, Sirota MG, Swadlow HA. 2003. Activity of different classes of neurons of the motor cortex during locomotion. J Neurosci. 23:1087–1097.

Betz V. 1874. Anatomischer Nachweis zweier Gehirncentra. Central-blatt fd Med Wissensch. 12:578–595.

Braitenberg VB, Schuz A. 1998. Cortex: statistics and geometry of neuronal connectivity. Berlin: Springer.

Calvin WH, Sypert GW. 1976. Fast and slow pyramidal tract neurons: an intracellular analysis of their contrasting repetitive firing properties in the cat. J Neurophysiol. 39:420–434.

Chattopadhyaya B, Di Cristo G, Higashiyama H, Knott GW, Kuhlman SJ, Welker E, Huang ZJ. 2004. Experience and activity-dependent maturation of perisomatic GABAergic innervation in primary visual cortex during a postnatal critical period. J Neurosci. 24:9598–9611.

Chen D, Fetz EE. 2005. Characteristic membrane potential trajectories in primate sensorimotor cortex neurons recorded in vivo. J Neurophysiol. 94:2713–2725.

Chen W, Zhang JJ, Hu GY, Wu CP. 1996a. Different mechanisms underlying the repolarization of narrow and wide action potentials in pyramidal cells and interneurons of cat motor cortex. Neuroscience. 73:57–68.

Chen W, Zhang JJ, Hu GY, Wu CP. 1996b. Electrophysiological and morphological properties of pyramidal and nonpyramidal neurons in the cat motor cortex in vitro. Neuroscience. 73:39–55.

Christophe E, Doerflinger N, Lavery DJ, Molnar Z, Charpak S, Audinat E. 2005. Two populations of layer v pyramidal cells of the mouse neocortex: development and sensitivity to anesthetics. J Neurophysiol. 94:3357–3367.

Dembrow NC, Chitwood RA, Johnston D. 2010. Projection-specific neuromodulation of medial prefrontal cortex neurons. J Neurosci. 30:16922–16937.

Deschenes M, Labelle A, Landry P. 1979. Morphological characterization of slow and fast pyramidal tract cells in the cat. Brain Res. 178:251–274.

Dykes RW, Lamour Y, Diadori P, Landry P, Dutar P. 1988. Somatosensory cortical neurons with an identifiable electrophysiological signature. Brain Res. 441:45–58.

Hattox AM, Nelson SB. 2007. Layer V neurons in mouse cortex projecting to different targets have distinct physiological properties. J Neurophysiol. 98:3330–3340.

Hooks BM, Hires SA, Zhang YX, Huber D, Petreanu L, Svoboda K, Shepherd GMG. 2011. Laminar analysis of excitatory local circuits in vibrissal motor and sensory cortical areas. PLoS Biol. 9: e1000572.

Ichinohe N, Watakabe A, Miyashita T, Yamamori T, Hashikawa T, Rockland KS. 2004. A voltage-gated potassium channel, Kv3.1b, is expressed by a subpopulation of large pyramidal neurons in layer 5 of the macaque monkey cortex. Neuroscience. 129: 179–185.

Isomura Y, Harukuni R, Takekawa T, Aizawa H, Fukai T. 2009. Microcircuitry coordination of cortical motor information in self-initiation of voluntary movements. Nat Neurosci. 12:1586–1593.

Kasper EM, Larkman AU, Lubke J, Blakemore C. 1994. Pyramidal neurons in layer 5 of the rat visual cortex. I. Correlation among cell morphology, intrinsic electrophysiological properties, and axon targets. J Comp Neurol. 339:459–474.

Katz LC, Burkhalter A, Dreyer WJ. 1984. Fluorescent latex microspheres as a retrograde neuronal marker for in vivo and in vitro studies of visual cortex. Nature. 310:498–500.

Kiritani T, Wickersham IR, Seung HS, Shepherd GMG. 2012. Hierarchical connectivity and connection-specific dynamics in the corticospinal-corticostriatal microcircuit in mouse motor cortex. J Neurosci. 32:4992–5001.

Kolkman KE, McElvain LE, du Lac S. 2011. Diverse precerebellar neurons share similar intrinsic excitability. J Neurosci. 31: 16665–16674.

Le Bé JV, Silberberg G, Wang Y, Markram H. 2007. Morphological, electrophysiological, and synaptic properties of corticocallosal pyramidal cells in the neonatal rat neocortex. Cereb Cortex. 17:2204–2213.

Li CX, Waters RS. 1991. Organization of the mouse motor cortex studied by retrograde tracing and intracortical microstimulation (ICMS) mapping. Can J Neurol Sci. 18:28–38.

Madeja M. 2000. Do neurons have a reserve of sodium channels for the generation of action potentials? A study on acutely isolated CA1 neurons from the guinea-pig hippocampus. Eur J Neurosci. 12:1–7.

Mason A, Larkman A. 1990. Correlations between morphology and electrophysiology of pyramidal neurons in slices of rat visual cortex: II. Electrophysiology. J Neurosci. 10:1415–1428.

Miller MN, Okaty BW, Nelson SB. 2008. Region-specific spike-frequency acceleration in layer 5 pyramidal neurons mediated by Kv1 subunits. J Neurosci. 28:13716–13726.

Morishima M, Kawaguchi Y. 2006. Recurrent connection patterns of corticostriatal pyramidal cells in frontal cortex. J Neurosci. 26:4394–4405.

Murray EA, Coulter JD. 1981. Organization of corticospinal neurons in the monkey. J Comp Neurol. 195:339–365.

Naito H, Nakamura K, Kurosaki T, Tamura Y. 1969. Precise location of fast and slow pyramidal tract cells in cat sensorimotor cortex. Brain Res. 14:237–239.

Nowak LG, Azouz R, Sanchez-Vives MV, Gray CM, McCormick DA. 2003. Electrophysiological classes of cat primary visual cortical neurons in vivo as revealed by quantitative analyses. J Neurophysiol. 89:1541–1566.

Nudo RJ, Masterton RB. 1990. Descending pathways to the spinal cord. III: sites of origin of the corticospinal tract. J Comp Neurol. 296:559–583.

Nudo RJ, Sutherland DP, Masterton RB. 1995. Variation and evolution of mammalian corticospinal somata with special reference to primates. J Comp Neurol. 358:181–205.

Oliva AA, Jr, Jiang M, Lam T, Smith KL, Swann JW. 2000. Novel hippocampal interneuronal subtypes identified using transgenic mice that express green fluorescent protein in GABAergic interneurons. J Neurosci. 20:3354–3368.

Petreanu L, Huber D, Sobczyk A, Svoboda K. 2007. Channelrhodopsin-2-assisted circuit mapping of long-range callosal projections. Nat Neurosci. 10:663–668.

Phillips CG, Porter R. 1977. Corticospinal neurones: their role in movement. London: Academic Press.

Preibisch S, Saalfeld S, Tomancak P. 2009. Globally optimal stitching of tiled 3D microscopic image acquisitions. Bioinformatics. 25:1463–1465.

Rathelot JA, Strick PL. 2006. Muscle representation in the macaque motor cortex: an anatomical perspective. Proc Natl Acad Sci USA. 103:8257–8262.

Rudy B, Fishell G, Lee S, Hjerling-Leffler J. 2011. Three groups of interneurons account for nearly 100% of neocortical GABAergic neurons. Dev Neurobiol. 71:45–61.

Rudy B, McBain CJ. 2001. Kv3 channels: voltage-gated K+ channels designed for high-frequency repetitive firing. Trends Neurosci. 24:517–526.

Sakai H, Woody CD. 1988. Relationships between axonal diameter, soma size, and axonal conduction velocity of HRP-filled, pyramidal tract cells of awake cats. Brain Res. 460:1–7.

Schuz A, Palm G. 1989. Density of neurons and synapses in the cerebral cortex of the mouse. J Comp Neurol. 286:442–455.

Schwindt PC, Spain WJ, Foehring RC, Stafstrom CE, Chubb MC, Crill WE. 1988. Multiple potassium conductances and their functions in neurons from cat sensorimotor cortex in vitro. J Neurophysiol. 59:424–449.

Sheets PL, Suter BA, Kiritani T, Chan CS, Surmeier DJ, Shepherd GMG. 2011. Corticospinal-specific HCN expression in mouse motor cortex: Ih-dependent synaptic integration as a candidate microcircuit mechanism involved in motor control. J Neurophysiol. 106:2216–2231.

Sheffield ME, Best TK, Mensh BD, Kath WL, Spruston N. 2011. Slow integration leads to persistent action potential firing in distal axons of coupled interneurons. Nat Neurosci. 14:200–207.

Spain WJ, Schwindt PC, Crill WE. 1991b. Two transient potassium currents in layer V pyramidal neurones from cat sensorimotor cortex. J Physiol. 434:591–607.

Spain WJ, Schwindt PC, Crill WE. 1991a. Post-inhibitory excitation and inhibition in layer V pyramidal neurones from cat sensorimotor cortex. J Physiol. 434:609–626.

Stefanis C, Jasper H. 1964. Intracellular microelectrode studies of antidromic responses in cortical pyramidal tract neurons. J Neurophysiol. 27:828–854.

Suter BA, O'Connor T, Iyer V, Petreanu LT, Hooks BM, Kiritani T, Svoboda K, Shepherd GMG. 2010. Ephus: multipurpose data acquisition software for neuroscience experiments. Front Neurosci Methods. 4:1–12.

Takahashi K. 1965. Slow and fast groups of pyramidal tract cells and their respective membrane properties. J Neurophysiol. 28:908–924.

Tanaka H, Ono K, Shibasaki H, Isa T, Ikenaka K. 2004. Conduction properties of identified neural pathways in the central nervous system of mice in vivo. Neurosci Res. 49:113–122.

Tanaka YH, Tanaka YR, Fujiyama F, Furata T, Yanagawa Y, Kaneko T. 2011. Local connections of layer 5 GABAergic interneurons to corticospinal neurons. Front Neural Circuits. 5:1–14.

Tennant KA, Adkins DL, Donlan NA, Asay AL, Thomas N, Kleim JA, Jones TA. 2011. The organization of the forelimb representation of the C57BL/6 mouse motor cortex as defined by intracortical microstimulation and cytoarchitecture. Cereb Cortex21:865–876.

Tseng GF, Parada I, Prince DA. 1991. Double-labelling with rhodamine beads and biocytin: a technique for studying corticospinal and other projection neurons in vitro. J Neurosci Methods. 37:121–131.

Tseng GF, Prince DA. 1993. Heterogeneity of rat corticospinal neurons. J Comp Neurol. 335:92–108.

Vigneswaran G, Kraskov A, Lemon RN. 2011. Large identified pyramidal cells in macaque motor and premotor cortex exhibit "thin spikes": implications for cell type classification. J Neurosci. 31:14235–14242.

Wang Y, Toledo-Rodriguez M, Gupta A, Wu C, Silberberg G, Luo J, Markram H. 2004. Anatomical, physiological and molecular properties of Martinotti cells in the somatosensory cortex of the juvenile rat. J Physiol. 561:65–90.

Weiler N, Wood L, Yu J, Solla SA, Shepherd GMG. 2008. Top-down laminar organization of the excitatory network in motor cortex. Nat Neurosci. 11:360–366.